Iterative Channel Estimation/Detection for DZT-OTFS Using Superimposed Pilot Frames

Vineetha Yogesh, Sandesh Rao Mattu, and A. Chockalingam
Department of ECE, Indian Institute of Science, Bangalore 560012

***Abstract*—Motivated by its inherent robustness to Doppler spread, Zak transform-based orthogonal time-frequency space (OTFS) modulation has emerged as a promising candidate for next-generation wireless technologies, particularly in the 6G and beyond framework. In this paper, we introduce a novel channel estimation algorithm for discrete Zak transform (DZT)-based OTFS, employing a superimposed pilot frame structure and capable of accommodating arbitrary pulse shapes and fractional delay-Dopplers (DD). The proposed algorithm leverages the DD channel invariance across multiple OTFS frames, which offers the benefit of multiple measurements in channel estimation. Extensive simulation results demonstrate that the proposed algorithm achieves good bit error rate (BER) and normalized mean square error (NMSE) performance, showcasing its effectiveness in practical communication settings. Impact of the use of different detectors on the iterative channel estimation/ detection performance is also studied.**

***Index Terms*—Discrete Zak transform, OTFS modulation, delay-Doppler domain, iterative channel estimation/detection, superimposed pilot.**

I. Introduction

Initial works on orthogonal time frequency space (OTFS) modulation viewed it as pre- and post-processing over the existing multicarrier modulation, i.e., orthogonal frequency division multiplexing (OFDM), which is referred to as multicarrier OTFS (MC-OTFS) [1], [2]. This approach to OTFS involves conversion of the DD domain symbols to intermediate time frequency (TF) domain before conversion to time domain for transmission. At the transmitter, inverse symplectic finite Fourier transform (ISFFT) is used to convert symbols from DD domain to TF domain, followed by Heisenberg transform for converting symbols from TF domain to time domain. The corresponding inverse transforms are used at the receiver. Just like Fourier transform provides a mathematical basis for frequency to time domain conversion and vice versa, Zak transform provides a mathematical framework to convert a DD domain signal directly to time domain and vice versa [3]. Zak transform for OTFS has been studied in the recent literature [1], [4]- [6]. In [4], the author considers continuous Zak transform based receiver, while the transmitter processing is still that of MC-OTFS. It shows that the spectral efficiency performance of the Zak receiver approach remains invariant to user velocity, whereas it degrades in OFDM as the velocity increases. In [5], the author provides a derivation of the complete OTFS transceiver based on continuous Zak transform from first principles and demonstrates its superior resilience to high Dopplers. The most recent Zak based OTFS works in [1] and [6] bring out the basic differences between MC-OTFS and Zak OTFS and shows the complete OTFS transceiver based on continuous Zak transform to have better resilience to large DD spreads. It also justifies why Zak based approach to OTFS is a natural fit to channels with large DD spreads and establishes its superiority over MC-OTFS, TDM, and FDM. However, the practical implementation of Zak based approach calls for a need for the discrete Zak transform (DZT) based approach [7]. In a related work, [8] studies OTFS using DZT (DZT-OTFS). The BER performance of DZT-OTFS is studied in [9] assuming perfect channel knowledge, which is compared with that of the MC-OTFS model in [4]. The works in [10]-[12] consider channel estimation in DZT-OTFS. While [10] considers an exclusive pilot frame for channel estimation, [11] and [12] consider two different approaches to channel estimation using embedded pilot frame. Both exhaustive and embedded pilot frames incur throughput loss due to pilot and guard symbols.

Superimposed pilot frames for channel estimation in MC-OTFS have been studied in [13]- [15]. In the superimposed pilot scheme in [13], both data and pilot symbols are superimposed in all the DD bins, and hence there is no loss in throughput. But this study assumes integer DDs and derives a minimum mean square error (MMSE) estimate of channel gains while assuming the perfect knowledge of path delays and Dopplers and the channel power delay profile. In [14], a sparse superimposed pilot frame structure is considered, where an MMSE estimate of channel gains is derived for integer DDs under the assumption that path delays and Dopplers are known. Optimum number of pilots and their placement is also studied. In [15], a single pilot superimposed in one of the bins in DD grid filled with data symbols is considered. The authors in [15] propose a threshold based channel estimator assuming integer Dopplers and fractional delays and a sum-product algorithm for data detection. To our knowledge, channel estimation for DZT-OTFS with superimposed pilot frames and fractional DDs is not studied in the literature so far.

In this paper, we consider the problem of channel estimation for DZT-OTFS using superimposed pilot frames in fractional DD channels and propose a novel algorithm for this purpose. The proposed algorithm cashes on the DD channel invariance across multiple OTFS frames, which offers the benefit of multiple measurements in channel estimation. Extensive simulation results are carried out to characterize the bit error rate (BER) and normalized mean square error

This work was supported in part by the J. C. Bose National Fellowship, Department of Science and Technology, Government of India. The first author would like to thank the Prime Minister's Research Fellowship, Ministry of Education, Government of India for the support.

(NMSE) performance of the algorithm. Our results demonstrate that the proposed algorithm achieves good BER and NMSE performance, showcasing its effectiveness in practical communication settings. We also study the impact of the use of different detectors on the iterative channel estimation/detection performance.

II. DZT-OTFS SYSTEM MODEL

In this section, the end-to-end DD domain input-output relation of the DZT-OTFS system with fractional DD and arbitrary transmit/receive pulse shape is derived. Information symbols $\mathbf{X}^{DD}[n,m]$ drawn from a modulation alphabet $\mathbb{A}$ is placed on the $N \times M$ DD grid defined as $\left\{ \left(n\Delta\nu = \frac{n}{NMT_s}, m\Delta\tau = mT_s \right), n = 0, \cdots, N-1, m = 0, \cdots, M-1 \right\}$, where T_s is the symbol duration, $\Delta\tau = T_s$ and $\Delta\nu = \frac{1}{NMT_s}$ are the resolutions along the delay and Doppler axis, respectively. $\mathbf{X}^{DD}[n,m]$ is converted to time domain using the inverse DZT (IDZT) [7], [8] as

$$\mathbf{x}^{TD}[u] = \frac{1}{\sqrt{N}} \sum_{n=0}^{N-1} \mathbf{X}^{DD}[n, u \bmod M] e^{j2\pi \frac{\lfloor u/M \rfloor}{N} n}. \quad (1)$$

After adding a cyclic prefix (CP) $U_{CP} > \lceil \tau_{\max}/T_s \rceil$ to $i)$ mitigate the inter-frame interference, $ii)$ convert liner convolution to circular convolution at the receiver after dropping CP, the resultant time domain sequence of length $NM + U_{CP}$ is mounted over the continuous time pulse $h_t(t);\ 0 \le t \le T_s$ to obtain a continuous time signal $x^{TD}(t);\ 0 \le t \le (NM + U_{CP})T_s$ given by

$$x^{TD}(t) = \sum_{u=0}^{NM+U_{CP}-1} \mathbf{x}^{TD}[(u - U_{CP})_{NM}] h_t(t - uT_s). \quad (2)$$

This signal then passes through a doubly-dispersive channel whose complex baseband channel response in DD domain is

$$c(\tau, \nu) = \sum_{i=1}^{P} c_i \delta(\tau - \tau_i)\delta(\nu - \nu_i), \quad (3)$$

where c_i, τ_i, and ν_i represent the ith path channel coefficient, delay, and Doppler, respectively. For fractional DD, $\frac{\tau_i}{\Delta\tau} = \eta_i = \alpha_i + a_i$ and $\frac{\nu_i}{\Delta\nu} = \zeta_i = \beta_i + b_i$, where α_i and β_i are the integer parts of the delay index and Doppler index, respectively, while $-\frac{1}{2} \le a_i, b_i \le \frac{1}{2}$ represent the corresponding fractional parts. The output of the time-varying channel is given by

$$y^{TD}(t) = \int_{\nu} \int_{\tau} c(\tau, \nu) x^{TD}(t - \tau) e^{j2\pi\nu(t-\tau)} d\tau d\nu + w(t), \quad (4)$$

where $w(t)$ is the additive white Gaussian noise (AWGN) added at the receiver. The resultant time domain signal is sampled at $t = kT_s$ after matched filtering (MF) with the receive pulse $h_r(t)$ to obtain the discrete time signal

$$\mathbf{y}^{MF}[k] = \sum_{i=1}^{P} c_i \sum_{u=0}^{NM-1} \mathbf{x}^{TD}[u] f[(k-u)T_s - \tau_i] e^{j2\pi\nu_i(\tau_+ nT_s)} + v[k], \quad (5)$$

where $f(t) \triangleq \int_{\tau} h(\tau) h^*(t - \tau) d\tau$ is the effective pulse obtained at the output of the MF, where $h(t) = h_t(t) = h_r(t)$, and $f[k]$ and $v[k]$ are the samples of $f(t)$ and $v(t)$, respectively, where $v(t)$ is the noise at the output of the MF. Simplifying (5) by substituting for τ_i and ν_i, we get the received vector $\mathbf{y}^{MF} \in \mathbb{C}^{1 \times NM}$ as

$$\mathbf{y}^{MF}[k] = \sum_{i=1}^{P} c_i e^{\frac{j2\pi\eta_i\zeta_i}{NM}} \sum_{u=0}^{NM-1} \mathbf{x}^{TD}[u] \mathbf{d}_i[u] \mathbf{f}_i[k-u] + \mathbf{v}[k] \quad (6)$$

$$= \sum_{i=1}^{P} c_i' \mathbf{y}_i^{MF}[k] + \mathbf{v}[k], \quad (7)$$

where $c_i' = c_i e^{\frac{j2\pi\eta_i\zeta_i}{N}}$, $\mathbf{f}_i[u] = \mathbf{f}[u - \eta_i]$, $\mathbf{d}_i[u] = e^{j2\pi\frac{\zeta_i}{NM}u}$, and $k, u = 0, \cdots, NM-1$. Here, $\mathbf{f}_i[u]$ and $\mathbf{d}_i[u]$ capture the effect of delay and Doppler of the ith path, respectively, and $\mathbf{y}_i^{MF}[k]$ is the component of received signal corresponding to the ith path, given by

$$\mathbf{y}_i^{MF}[m] = \sum_{u=0}^{NM-1} \mathbf{x}^{TD}[u] \mathbf{d}_i[u] \mathbf{f}_i[k-u]. \quad (8)$$

At the receiver, $\mathbf{y}^{MF}$ is converted to DD domain using DZT as

$$\mathbf{Y}^{DD}[n,m] = \frac{1}{\sqrt{N}} \sum_{u=0}^{N-1} \mathbf{y}^{MF}[m + uM] e^{-j2\pi\frac{n}{N}u}. \quad (9)$$

The equivalent DD domain representations of (7) and (8) are

$$\mathbf{Y}^{DD}[n,m] = \sum_{i=1}^{P} c_i' \mathbf{Y}_i^{DD}[n,m] + \mathbf{V}^{DD}[n,m], \quad (10)$$

$$\mathbf{Y}_i^{DD}[n,m] = \sum_{l=0}^{M-1} \sum_{k=0}^{N-1} \mathbf{X}^{DD}[k,l] \mathbf{D}_i^{DD}[n-k, l] \mathbf{F}_i^{DD}[k, m-l], \quad (11)$$

respectively, where $\mathbf{D}_i^{DD}$, $\mathbf{F}_i^{DD}$, and $\mathbf{V}^{DD}$ are the DZT of the sequences $\mathbf{d}_i$, $\mathbf{f}_i$, and $\mathbf{v}$, respectively.

A. Vectorized input-output relation

Further, for vectorizing (10), let $\mathbf{A}_m$ be a $N \times N$ matrix whose jth row is $\mathbf{A}_m[j-1,:] = (\mathbf{D}_i^{DD}[:, m-1])^T \mathbf{P}_N^{j-1}$, where $m = 1, \cdots, M$, $j = 1, \cdots, N$, and $\mathbf{P}_N$ is a $N \times N$ basic circulant permutation matrix (BCPM) [17]. Next, define block diagonal matrix $\mathbf{D}_i$ with matrices $\{\mathbf{A}_m\}_{m=1}^{M}$ along the diagonal. Likewise, define a $N \times N$ block matrix $\mathbf{B} = [\text{diag}\{\mathbf{F}_i^{DD}[:,0]\}, \cdots, \text{diag}\{\mathbf{F}_i^{DD}[:, M-1]\}]$. Let $\mathbf{Q}_m = \mathbf{P}_M^{m-1} \otimes \mathbf{I}_N$ be an $NM \times NM$ matrix, where $\mathbf{P}_M$ is an $M \times M$ BCPM and $\otimes$ operator denotes Kronecker product.

Also, define an $NM \times NM$ matrix $\mathbf{F}_i = \begin{bmatrix} \mathbf{BQ}_1 \\ \vdots \\ \mathbf{BQ}_M \end{bmatrix}$. Using $\mathbf{D}_i$ and $\mathbf{F}_i$, the effective channel matrix $\mathbf{H}$ in DD domain can be written as

$$\mathbf{H} = \sum_{i=1}^{P} c_i' \mathbf{D}_i \mathbf{F}_i. \tag{12}$$

Note that, since $\mathbf{F}_i$s capture the effect of delays (η_is) and $\mathbf{D}_i$s capture the effect of Dopplers (ζ_is), the channel representation in (12) is in a form that decouples the effect of channel gains (c_is), delays (η_is), and Dopplers (ζ_is). This decoupled representation is instrumental in devising the low complexity algorithm proposed in Sec. III. Finally, (10) can be written as

$$\mathbf{y}_{\text{DD}} = \mathbf{x}_{\text{DD}}\mathbf{H} + \mathbf{v}_{\text{DD}}, \tag{13}$$

where $\mathbf{y}_{\text{DD}} = vec(\mathbf{Y}^{DD}), \mathbf{x}_{\text{DD}} = vec(\mathbf{X}^{DD})$, and $\mathbf{v}_{\text{DD}} = vec(\mathbf{V}^{DD}) \in \mathbb{C}^{1\times N}$, where, $vec(\cdot)$ denotes column-wise vectorization of matrix and $unvec(\cdot)$ denotes the inverse operation.

III. Proposed channel estimation algorithm

For the purpose of data detection, an estimate of the channel $\mathbf{H}$ is required at the receiver. To enable the channel estimation, a known symbol called pilot is transmitted as a part of the OTFS frame. There are different frame structures such as i) exclusive pilot frame (an entire OTFS frame is dedicated for the pilot, and data is transmitted over the consecutive OTFS frames), and ii) embedded pilot frame (both data and pilot are present in a frame, and the pilot is surrounded by a guard band to mitigate interference between pilot and data). Both the above frame structures suffer loss in spectral efficiency. Hence, in this paper a superimposed pilot scheme is considered. In this superimposed pilot scheme, the entire OTFS frame is filled with data symbols. In addition, pilot symbols are superimposed on select locations. The superimposed pilot frame structure considered in this paper is defined below.

A. Superimposed pilot frame structure

The OTFS frame is filled with NM data symbols $x_d \in \mathbb{A}$. In addition, one pilot symbol with amplitude x_p is mounted on top of the one of the data symbols at the selected location in the DD grid, denoted by (n_p, m_p). Fig. 1 shows the superimposed pilot frame structure considered in this paper, which can be written as

$$\mathbf{X}^{DD}[n,m] = \mathbf{X}_d[n,m] + \mathbf{X}_p[n,m], \tag{14}$$

$$\mathbf{X}_p[n,m] = \begin{cases} x_p \ ; \ n = n_p, m = m_p \\ 0 \quad ; \text{otherwise}, \end{cases} \tag{15}$$

and $\mathbf{X}_d[n,m] = x_d \ \forall n \in [0, N-1], m \in [0, M-1]$.

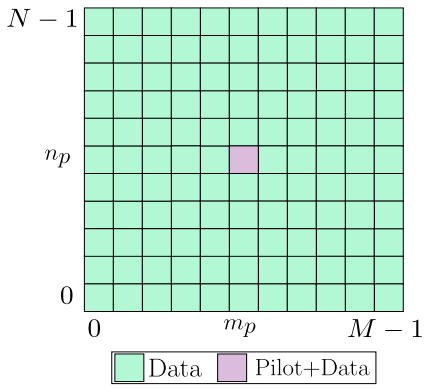

Fig. 1: Superimposed pilot frame structure.

B. Proposed channel estimation algorithm

The proposed algorithm is iterative in nature. In each iteration, channel estimation followed by channel equalization and data detection is performed. The proposed algorithm is described as follows. Using (14) in (13), the contributions of data and pilot symbols in the received DD domain signal can be separated as

$$\mathbf{y}_{\text{DD}} = \mathbf{x}_p\mathbf{H} + \mathbf{x}_d\mathbf{H} + \mathbf{v}_{\text{DD}}, \tag{16}$$

where $\mathbf{x}_{\text{DD}} = \mathbf{x}_p + \mathbf{x}_d$, $\mathbf{x}_p$ and $\mathbf{x}_d$ are obtained as $vec(\mathbf{X}_p)$ ans $vec(\mathbf{X}_d)$, respectively. In (16), $\mathbf{x}_d\mathbf{H}$ is the contribution of data symbols in the received OTFS frame and $\mathbf{x}_p\mathbf{H}$ is the contribution of pilot. Note that there is significantly high interference from the data symbols present in the frame to the pilot. This hinders the channel estimation which in turn affects the BER performance of the system. To mitigate the interference from the data symbols in the OTFS frame, we propose the following algorithm.

1) Interference (data + noise) cancellation through averaging: The data symbols x_ds are drawn independently and uniformly from $\mathbb{A}$ whose mean is zero. Taking expectation on (16), under the assumption that the DD channel is invariant,

$$\begin{aligned} \mathbb{E}[\mathbf{y}_{\text{DD}}] &= \mathbb{E}[\mathbf{x}_p\mathbf{H}] + \mathbb{E}[\mathbf{x}_d\mathbf{H}] + \mathbb{E}[\mathbf{v}_{\text{DD}}] \\ &= \mathbf{x}_p\mathbf{H}, \end{aligned} \tag{17}$$

where the $\mathbf{v}_{\text{DD}}$ samples are from zero mean AWGN process. In practice, $\mathbb{E}[\mathbf{y}_{\text{DD}}]$ can be obtained by using the time average of the received DD frame, assuming channel is invariant over I OTFS frames, as

$$\mathbb{E}[\mathbf{y}_{\text{DD}}] \approx \frac{1}{I}\sum_{i=1}^{I} \mathbf{y}_{\text{DD}}^i, \tag{18}$$

where $\{\mathbf{y}_{\text{DD}}^i\}_{i=1}^I$ are I consecutive received OTFS frames. Note that (18) becomes increasingly accurate for large I. The choice of I in practical scenarios depends on the spatial coherence of the channel in the DD domain (e.g., [16] assumes that the scattering environment and DD channel gains are invariant over 20 OTFS frames). When I is small, the averaging in (18) becomes less accurate, in which case iterations between channel estimation and detection as described below can improve performance.

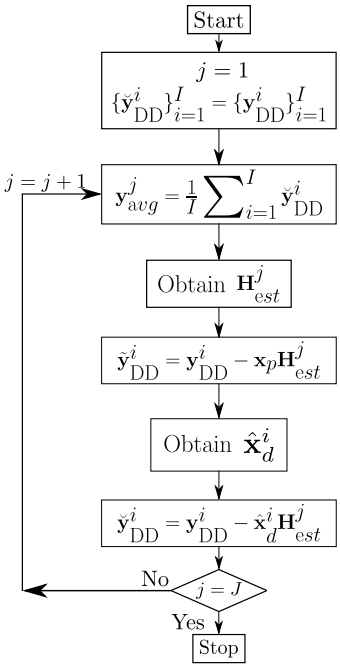

Fig. 2: Proposed iterative channel estimation/detection algorithm.

Let $\{\breve{\mathbf{y}}^i_{\text{DD}}\}_{i=1}^I = \{\mathbf{y}^i_{\text{DD}}\}_{i=1}^I$. In the first channel estimation/detection iteration, i.e., $j=1$, obtain $\mathbf{y}^j_{avg} = \frac{1}{I}\sum_{i=1}^I \breve{\mathbf{y}}^i_{\text{DD}}$. The algorithm described in Sec. III-B2 (channel estimation algorithm proposed for embedded pilot frame in [12] modified and adopted) is used to obtain an estimate of the effective channel matrix, i.e., $\mathbf{H}^j_{est}$. Next, for the ith frame ($i \in [1,\cdots,I]$), the contribution of the pilot is removed from received frame $\mathbf{y}^i_{\text{DD}}$ to obtain $\tilde{\mathbf{y}}^i_{\text{DD}}$ as

$$\tilde{\mathbf{y}}^i_{\text{DD}} = \mathbf{y}^i_{\text{DD}} - \mathbf{x}_p\mathbf{H}^j_{est}. \tag{19}$$

Further, $\tilde{\mathbf{y}}^i_{\text{DD}}$ is used to obtain the detected data symbols denoted as $\hat{\mathbf{x}}^i_d$. The $\breve{\mathbf{y}}^i_{\text{DD}}$ is then updated by cancelling the data interference as

$$\breve{\mathbf{y}}^i_{\text{DD}} = \mathbf{y}^i_{\text{DD}} - \hat{\mathbf{x}}^i_d\mathbf{H}^j_{est}. \tag{20}$$

An average for the subsequent iteration is computed as $\mathbf{y}^{j+1}_{avg} = \frac{1}{I}\sum_{i=1}^I \breve{\mathbf{y}}^i_{\text{DD}}$. This completes one iteration of proposed algorithm. The algorithm terminates when $j=J$, where J is the maximum number of iterations.

2) Obtaining $\mathbf{H}^j_{est}$: The algorithm proceeds iteratively estimating channel coefficients, delay and Doppler for each path (strongest path first) and successively removing the effect of estimated path from $\mathbf{y}^j_{avg}$ before going on to estimate the next strongest path. The strength of the path is measured by the energy in received frame. The iterations start by initializing $p=1$ and continue till $p=P_{\max}$ or till the bin energy in the received frame after successively removing the contributions of estimated paths reduces to that of the interference (noise + data) floor, i.e, based on a stopping criteria. Here note that, P' paths are estimated where $P' \geq P$ and $P' \leq P_{\max}$. Estimating $P' \geq P$ is necessary since i) number of paths P in the channel is unknown and ii) due fractional DD nature, there is a considerable spillover of the path energy over the adjacent DD bins along both delay and Doppler. Assuming data is absent, a maximum likelihood (ML) estimate of channel gain is obtained as a function of path delay and Doppler as

$$\hat{c}_p(\hat{\eta}_p,\hat{\zeta}_p) = \frac{\mathbf{Y}^j_{\text{avg}}[n^p_r, m^p_r]}{\boldsymbol{\varphi}_{\hat{\eta}_p,\hat{\zeta}_p}[Nm^p_r + n^p_r]}, \tag{21}$$

where (n^p_r, m^p_r) is the maximum energy location in $\mathbf{Y}^j_{avg}$ in pth iteration (see **Step 1** below), $\boldsymbol{\varphi}_{\hat{\eta}_p,\hat{\zeta}_p} = \mathbf{x}_p\hat{\mathbf{D}}_p(\hat{\zeta}_p)\hat{\mathbf{F}}_p(\hat{\eta}_p)$, with $\hat{\mathbf{F}}_p(\hat{\eta}_p)$ and $\hat{\mathbf{D}}_p(\hat{\beta}_p)$ computed by using the estimated delay and Doppler indices $\hat{\eta}_p$ and $\hat{\zeta}_p$ in $\mathbf{F}_i$ and $\mathbf{D}_i$, respectively. The steps involved in obtaining the estimates $\{\hat{c}_p,\hat{\eta}_p,\hat{\zeta}_p\}_{p=1}^{P'}$ are described below. Start by initializing $p=1$.

Step 1 : Coarse estimates of DD

Let $\mathbf{Y}^j_{avg}$ be the $N \times M$ matrix obtained as *unvec*($\mathbf{y}^j_{avg}$). Let $\mathbf{Y}^{j,p}_{avg} = \mathbf{Y}^j_{avg}$ the maximum energy location in $\mathbf{Y}^{j,p}_{avg}$ be denoted by (n^p_r, m^p_r), i.e., $(n^p_r, m^p_r) = \arg\max_{n,m} |\mathbf{Y}^{j,p}_{avg}[n,m]|^2$. Then the coarse estimate (denoted by superscript c) of delay and Doppler of pth path is $\hat{\eta}^c_p = m^p_r - m_p$ and $\hat{\zeta}^c_p = n^p_r - n_p$, respectively.

Step 2 : Refining delay estimate by correlating the received signal on delay axis with $f(t)$

In this step, a fractional estimate of the delay index (η_p) is obtained using the knowledge of $\hat{\eta}^c_p$ as follows. For the pth path, the L1-norm is minimized between the normalized received vector and the MF response vector of lengths $2q+1$ centered around their respective maximum amplitude locations, where q is the number of bins on either side of the maximum amplitude location. These $(2q+1)$-length vectors are called *normalized adjacent bin level (NABL) vectors*. The received NABL vector is denoted by $\mathbf{y}^p_{\text{NABL}}$, obtained as $\mathbf{y}^p_{\text{NABL}} = \frac{[\breve{\mathbf{Y}}^{j,p}_{avg}[n^p_r, m^p_r - q], \breve{\mathbf{Y}}^{j,p}_{avg}[n^p_r, m^p_r - q+1] \cdots \breve{\mathbf{Y}}^{j,p}_{avg}[n^p_r, m^p_r + q]]}{\breve{\mathbf{Y}}^{j,p}_{avg}[n^p_r, m^p_r]}$ where $\breve{\mathbf{Y}}^{j,p}_{avg} = |\mathbf{Y}^{j,p}_{avg}|$. The MF response NABL vector, denoted by $\mathbf{f}_{\text{NABL}}$, is obtained as follows. The delays around $\hat{\eta}^c_p$ for fine search is defined as $\mathcal{L} = \{\hat{\eta}^c_p - 0.5, \hat{\eta}^c_p - 0.5 + \Delta_\eta, \hat{\eta}^c_p - 0.5 + 2\Delta_\eta, \cdots, \hat{\eta}^c_p + 0.5\}$, where Δ_η is the delay search resolution. For each $\mathcal{L}(l)$, $f(t;\mathcal{L}(l))$ is obtained by delaying $f(t)$ by $\mathcal{L}(l)T_s$, which on sampling at T_s intervals (i.e., $t = uT_s$) yields $\mathbf{f}[u;\mathcal{L}(l)]$, where $u = 0,1,\cdots,NM-1$. Now, for each $\mathbf{f}[u;\mathcal{L}(l)]$, the location of maximum amplitude is obtained as $k = \arg\max_u \breve{\mathbf{f}}[u;\mathcal{L}(l)]$. Next, the $\mathbf{f}_{\text{NABL}}(\mathcal{L}(l))$ vector is obtained by picking q values on either side of k as $\mathbf{f}_{\text{NABL}}(\mathcal{L}(l)) = \frac{[\breve{\mathbf{f}}[k-q;\mathcal{L}(l)]\ \breve{\mathbf{f}}[k-q+1;\mathcal{L}(l)] \cdots \breve{\mathbf{f}}[k+q;\mathcal{L}(l)]]}{\breve{\mathbf{f}}[k;\mathcal{L}(l)]}$ where, $\mathbf{f}[u;\breve{\mathcal{L}}(l)] = |\mathbf{f}[u;\mathcal{L}(l)]|$ Finally, a minimization of $\|\mathbf{y}^p_{\text{NABL}} - \mathbf{f}_{\text{NABL}}(\mathcal{L}(l))\|_1$ is performed over $\mathcal{L}(l)$ to obtain $\tilde{\eta}^f_p$. Through simulations, it is observed that $q=1$ attains the best NMSE and BER performance. Also, through simulations it is observed that L1-norm gives more robust estimation compared to L2-norm. Hence, we adopt $q=1$ and L1-norm in all the simulations.

Step 3 : Refining Doppler estimate - ML estimation

The estimated $\tilde{\eta}^f_p$ (superscript f denotes fine estimate) is

used to obtain $\hat{\zeta}_p^f$ as follows. The Doppler search area is defined as $\mathcal{G} = \{\hat{\zeta}_p^c - 0.5, \hat{\zeta}_p^c - 0.5 + \Delta_\zeta, \hat{\zeta}_p^c - 0.5 + 2\Delta_\zeta, \cdots, \hat{\zeta}_p^c + 0.5\}$, where Δ_ζ is the Doppler search resolution. For each $\rho_l \in \mathcal{G}$, $l = 1, 2, \cdots, \overline{\overline{\mathcal{G}}}$, the channel coefficients $(c_i(\tilde{\eta}_p^f, \rho_l))$ are computed using (21) (with $\hat{\eta}_p = \tilde{\eta}_p^{(f)}$, $\hat{\zeta}_p = \rho_l$), followed by the computation of the channel matrix, $\hat{\mathbf{H}}(\tilde{\eta}_p^{(f)}, \rho_l, c_i(\tilde{\eta}_p^f, \rho_l))$ using (12). An ML estimate of Doppler is obtained by maximizing the log-likelihood function over $\mathcal{G}$, i.e., $\arg\max_{\rho_l \in \mathcal{G}} \log(P(\mathbf{y}_{avg}^{j,p} | \hat{\mathbf{H}}(\tilde{\eta}_p^{(f)}, \rho_l, c_i(\tilde{\eta}_p^f, \rho_l)), \mathbf{x}_p))$, which is equivalent to

$$\hat{\zeta}_p^f = \arg\min_{\rho_l \in \mathcal{G}} \left\| \mathbf{y}_{avg}^{j,p} - \mathbf{x}_p \hat{\mathbf{H}}(\tilde{\eta}_p^{(f)}, \rho_l, c_i(\tilde{\eta}_p^f, \rho_l)) \right\|_2, \quad (22)$$

where $P(\mathbf{y}_{avg}^{j,p} | \hat{\mathbf{H}}, \mathbf{x}_p) \sim \mathcal{CN}(\mathbf{x}_p \hat{\mathbf{H}}, \sigma^2 \mathbf{I})$, $\sigma^2 \mathbf{I}$ is the $N \times N$ covariance matrix of noise ($\mathbf{v}_{\text{DD}}$), and $\| \cdot \|_2$ is vector 2-norm.

Step 4 : Re-refining delay estimate - ML estimation
This $\hat{\zeta}_p^f$ is used to obtain a refined delay estimate $\hat{\eta}_p^f$. As described above, an ML estimate of delay is obtained in (23), where the search is carried over $\mu_l \in \mathcal{L}$, for $l = 1, 2, \cdots, \overline{\overline{\mathcal{L}}}$ ($\bar{\cdot}$ denotes cardinality of a set). For each μ_l, the channel coefficients $c_i(\mu_l, \hat{\zeta}_p^f)$ are computed using (21) (with $\hat{\eta}_p = \mu_l$, $\hat{\zeta}_p = \hat{\zeta}_p^f$), followed by the computation of the channel matrix, $\hat{\mathbf{H}}(\mu_l, \hat{\zeta}_p^{(f)}, c_i(\mu_l, \hat{\zeta}_p^f))$, and $\hat{\eta}_p^{(f)}$ is obtained as

$$\hat{\eta}_p^f = \arg\min_{\mu_l \in \mathcal{J}} \left\| \mathbf{y}_{avg}^{j,p} - \mathbf{x}_p \hat{\mathbf{H}}(\mu_l, \hat{\zeta}_p^{(f)}, c_i(\mu_l, \hat{\zeta}_p^f)) \right\|_2. \quad (23)$$

The fine estimate of channel coefficient $\hat{h}_i^{(f)}$ is obtained using (21). We note that while $\tilde{\alpha}_i^{(f)}$ is an initial estimate, $\hat{\alpha}_i^{(f)}$ is a refined estimate, refined using the knowledge of $\hat{\beta}_i^{(f)}$ and $h_i^{(c)}$ in (23), and the refinement helps to improve performance.

Step 5 : Inter-path interference (IPI) cancellation
The effect of pth estimated path is removed from $\mathbf{Y}_{avg}^{j,p}$. To do this, the channel matrix for the pth path, $\mathbf{H}_{est}^{j,p}(\hat{\eta}_p^{(f)}, \hat{\zeta}_p^{(f)}, \hat{c}_p^{(f)})$ is constructed. The pth path's estimated contribution is $\hat{\mathbf{y}}_{est,p} = \mathbf{x}_p \mathbf{H}_{est}^{j,p}(\hat{\eta}_p^{(f)}, \hat{\zeta}_p^{(f)}, \hat{c}_p^{(f)})$. Next, $\mathbf{Y}_{est,p}$ obtained as *unvec*$(\mathbf{y}_{est,p})$ is used for IPI cancellation as

$$\mathbf{Y}_{avg}^{j,p+1} = \mathbf{Y}_{avg}^{j,p} - \mathbf{Y}_{est,p}, \quad (24)$$

and $\mathbf{Y}_{avg}^{j,p+1}$ is used in **Steps 1-4** to estimate the channel parameters for the $(p+1)$th path.

Step 6 : Stopping criteria
The algorithm stops at the pth iteration if either $p = P_{\max}$ or $\left| \|\mathbf{Y}_{avg}^{j,p}\|_F - \|\mathbf{Y}_{avg}^{j,p-1}\|_F \right| \leq \epsilon^j$, where ϵ^j is the convergence parameter for the jth iteration.

Once the algorithm terminates after estimating P' paths, the vector of estimated delays, Dopplers, and channel coefficients are used to construct the estimated channel matrix $\mathbf{H}_{est}^j$ using (12).

IV. Results and Discussions

In this section, we present the NMSE and BER performance obtained using the proposed estimation algorithm for different pulse shapes and detectors. An OTFS frame of size $N = 16$ and $M = 48$ is considered for this purpose and total available bandwidth is $B = 200$ kHz. The Delay and Doppler spreads of the channel are $\tau_{\max} = 20$ μs and $\nu_{\max} = 781.25$ Hz, respectively. The channel is assumed to have $P = 4$ paths with uniform power delay profile (PDP). The delays of the paths are assumed to be uniformly distributed in $[0, \tau_{\max}]$ and the Dopplers of the paths are assumed to have uniform distribution in $[-\nu_{\max}, \nu_{\max}]$. The following algorithm parameters are used: $I = 5, 20$, $J = 6$, $(n_p, m_p) = (N/2, M/2)$, $P_{\max} = 15$, $\Delta_\eta = \Delta_\zeta = 0.01$. Results are provided for transmit and receive pulse being i) square-root raised cosine (SRRC) pulse with roll off factor $\gamma = 0.5$, i.e., $h(t) = \frac{\sin(\pi(1-\gamma)t/T_s) + 4\gamma(t/T_s)\cos(\pi(1+\gamma)t/T_s)}{\pi(t/T_s)(1-(4\gamma(t/T_s))^2)}$ (where $f(t)$ is raised cosine pulse), and ii) rectangular pulse given by $h(t) = \begin{cases} 1/\sqrt{T_s}; 0 \leq t \leq T_s \\ 0 \quad ; \text{otherwise} \end{cases}$ (where $f(t)$ is triangular pulse). 4-QAM modulation alphabet is considered. MMSE detector and message passing (MP) detector [18] are employed. Pilot signal to noise ratio (SNR) is considered to be same as data SNR.

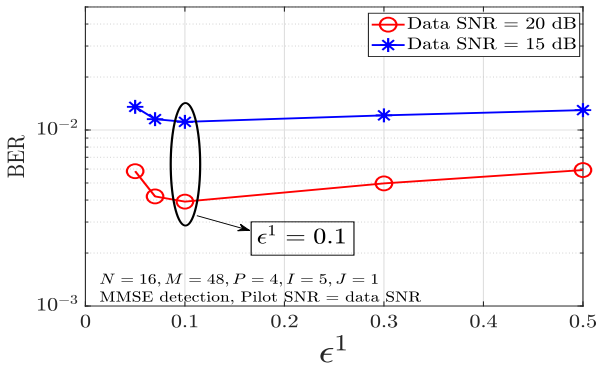

Fig. 3: BER performance as a function of ϵ^1.

1) Choice of convergence parameter: The choice of convergence parameter ϵ^j for jth iteration is crucial since it decides the number of estimated paths P'. A very small value of ϵ^j could imply that noise may be estimated as a valid path, while a large value of ϵ^j may imply that $P' < P$ paths are estimated. The value of convergence factor depends on the residual interference (data + noise) floor. With small I, there will be significant data residue in $j = 1$th iteration. However, in subsequent iterations, the interference floor is mostly governed by noise statistics only owing to data interference cancellation and averaging. Hence, it is expected that $\epsilon^1 \geq \epsilon^j; j \neq 1$. Simulation results are found to corroborate this observation as seen in Fig. 3, which shows BER as a function of ϵ^1 for data SNR = 20 dB and 15 dB. For $I = 5$, it is observed that $\epsilon^1 = 0.1$ is optimum. Similar study for $\epsilon^j, j \neq 1$ showed that $\epsilon^j = 0.01$ is optimum. In all the simulations with $I = 5$, $\epsilon^1 = 0.1$ and $\epsilon^j = 0.01 \, \forall j \neq 1$ are considered. For $I = 20$, $\epsilon^j = 0.01 \, \forall j$.

2) NMSE performance of proposed algorithm: NMSE in iteration jth is computed as $\frac{\|\mathbf{H} - \mathbf{H}_{est}^j\|_F^2}{\|\mathbf{H}\|_F^2}$. Figure 4 shows the

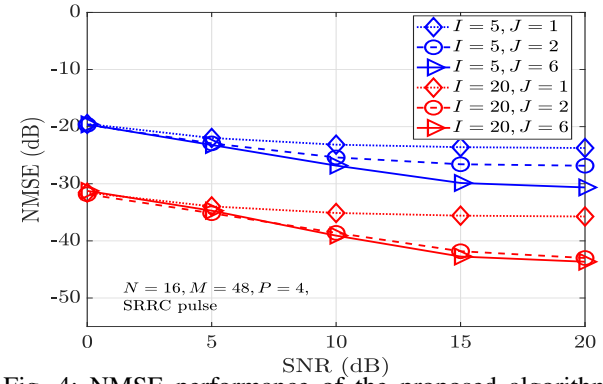

Fig. 4: NMSE performance of the proposed algorithm as a function of I and J.

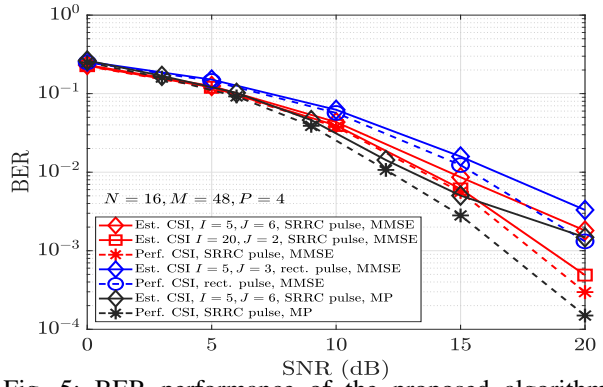

Fig. 5: BER performance of the proposed algorithm as a function of SNR.

NMSE performance of the proposed algorithm as a function of SNR (data SNR) for different values of I and J for SRRC pulse. $I = 5, 20$ and $J = 1, 2, 6$ are considered. For $I = 5$, the performance improvement is marginal after $J = 6$, while in case of $I = 20$, the performance gain is marginal just after $J = 2$. It is observed that as I increases, the maximum number of iterations (J) required decreases. This is attributed to effective data interference cancellation due to averaging.

3) BER performance of proposed algorithm: Figure 5 shows the BER performance of the proposed algorithm as a function of SNR with different transmit pulse shapes, for two detectors, namely, MMSE and MP detectors. The performance obtained using the estimated channel is compared against that obtained using the perfect channel knowledge. BER performance using MMSE detector is obtained for SRRC pulse for $I = 5, 20$ and rectangular pulse for $I = 5$. The BER performance for SRRC pulse is also obtained using MP detector with $I = 5$. It is observed that the performance obtained using both perfect channel knowledge and estimated channel knowledge with MP detector is superior over that obtained using MMSE detector. Also, the performance obtained using SRRC pulse is superior compared to that obtained using the rectangular pulse, owing to better spectral characteristics of the SRRC pulse.

V. Conclusion

In this work, we presented a novel iterative channel estimation/detection algorithm for DZT-OTFS utilizing superimposed pilot frames. Leveraging the inherent DD domain channel invariance over multiple OTFS frames, the proposed algorithm effectively mitigates data and pilot interference. We analyzed the impact of statistical channel characteristics on performance (e.g., impact of number of frames over which the DD channel remains invariant). Additionally, we investigated the effect of different detection algorithms (MMSE and MP detection algorithms) within the iterative channel estimation/detection framework. Simulation results demonstrated that the proposed algorithm not only achieves superior NMSE performance but also a BER performance that is close to that obtained using perfect channel state information, while achieving full spectral efficiency.

References

[1] S. K. Mohammed, R. Hadani, A. Chockalingam, and R. Calderbank, "OTFS - a mathematical foundation for communication and radar sensing in the delay-Doppler domain," *IEEE BITS the Information Theory Magazine*, vol. 2, no. 2, pp. 36-55, Nov. 2022.

[2] Z. Wei et al., "Orthogonal time-frequency space modulation: a promising next-generation waveform," *IEEE Wireless Commun. Mag.*, vol. 28, no. 4, pp. 136-144, Aug. 2021.

[3] A. J. E. M. Janssen, "The Zak transform: a signal transform for sampled time-continuous signals," *Philips J. Res.*, 43, pp. 23-69, 1988.

[4] S. K. Mohammed, "Time-domain to delay-Doppler domain conversion of OTFS signals in very high mobility scenarios," *IEEE Trans. Veh. Tech.,* vol. 70, no. 6, pp. 6178-6183, Jun. 2021.

[5] S. K. Mohammed, "Derivation of OTFS modulation from first principles," *IEEE Trans. Veh. Tech.,* vol. 70, no. 8, pp. 7619-7636, Aug. 2021.

[6] S. K. Mohammed, R. Hadani, A. Chockalingam, and R. Calderbank, "OTFS - predictability in the delay-Doppler domain and its value to communication and radar sensing," *IEEE BITS the Information Theory Magazine*, IEEE early access, doi: 10.1109/MBITS.2023.3319595.

[7] H. Bolcskei and F. Hlawatsch, "Discrete Zak transforms, polyphase transforms, and applications," *IEEE Trans. Signal Process.*, vol. 45, no. 4, pp. 851-866, Apr. 1997.

[8] F. Lampel, A. Avarado and F. M. J. Willems, "On OTFS using the discrete Zak transform," *Proc. IEEE ICC'2022 Workshops*, pp. 729-734, May 2022.

[9] V. Yogesh, V. Bhat, S. R. Mattu, and A. Chockalingam, "On the bit error performance of OTFS modulation using discrete Zak transform," *Proc. IEEE ICC'2023*, pp. 741-746, May-Jun. 2023.

[10] S. P. Muppaneni, S. R. Mattu, and A. Chockalingam, "Delay-Doppler domain channel estimation for DZT-based OTFS systems," *Proc. IEEE SPAWC'2023*, pp. 236-240, Sep. 2023.

[11] S. P. Muppaneni, S. R. Mattu, and A. Chockalingam, "Data-aided fractional delay-Doppler channel estimation with embedded pilot frames in DZT-based OTFS," *Proc. IEEE VTC'2023-Fall*, pp. 1-7, Oct. 2023.

[12] V. Yogesh, S. R. Mattu, and A. Chockalingam, "Low-complexity delay-Doppler channel estimation in discrete Zak transform based OTFS," *IEEE Commun. Lett.*, IEEE early access, doi: 10.1109/LCOMM.2024.3351685.

[13] H. B. Mishra *et al.*, "OTFS channel estimation and data detection designs with superimposed pilots," *IEEE Trans. Wireless Commun*, vol. 21, no. 4, pp. 2258-2274, Apr. 2022.

[14] F. Jesbin, S. R. Mattu and A. Chockalingam, "Sparse superimposed pilot based channel estimation in OTFS systems," *IEEE WCNC'2023*, pp. 1-6, Mar. 2023,

[15] W. Yuan *et al.*, "Data-aided channel estimation for OTFS systems with a superimposed pilot and data transmission scheme," *IEEE Wireless Commun. Lett.*, vol. 10, no. 9, pp. 1954-1958, Sep. 2021

[16] M. Li *et al.*, "Joint channel estimation and data detection for hybrid RIS aided millimeter wave OTFS systems," *IEEE Trans. Commun.*, vol. 70, no. 10, pp. 6832-6848, Oct. 2022.

[17] R. Horn and C. Johnson, *Matrix Analysis*, Cambridge Univ. Press, 2013.

[18] P. Raviteja, K. T. Phan, Y. Hong, and E. Viterbo, "Interference cancellation and iterative detection for orthogonal time frequency space modulation," *IEEE Trans. Wireless Commun.,* vol. 17, no. 10, pp. 6501-6515, Aug. 2018.